

# Direct numerical simulation benchmarks for the prediction of boundary-layer bypass transition in the narrow sense

By C. A. Gonzalez, R. Agrawal, X. Wu<sup>†</sup> AND P. Moin

We perform and report statistics from direct numerical simulations of bypass transition in the narrow sense with inlet freestream turbulence intensity levels of 0.75%, 1.5%, 2.25%, 3.0% and 6.0%, respectively. An intermittency correlation formula is proposed and compared with data from the literature, and the classical Abu-Ghannam and Shaw correlation is found to describe the beginning, rather than the completion, of the late transitional stage. Accompanying Reynolds-averaged Navier-Stokes simulations are performed and found to be highly sensitive to modeling parameters in the turbulence closure model.

---

## 1. Introduction

Engineers have strong and sustained interests in predicting the location of boundary-layer transition in the flows over aircraft wings, jet-engine turbofan airfoils, compressors, and turbine blades. Transition modeling has remained an active research field over the past half-century. Representative approaches for engineering transition prediction include data correlations, Reynolds-averaged Navier-Stokes (RANS) turbulence models, a RANS turbulence model coupled with an intermittency equation, a stand-alone intermittency equation, and laminar fluctuation energy (for additional details, see Dick & Kubacki (2017) and Durbin (2018)).

### 1.1. Motivation for benchmarking transition prediction

An important step in transition prediction is the evaluation of the predictive ability of a given RANS/correlation model in a zero-pressure-gradient, smooth-wall, flat-plate boundary layer under isotropic freestream turbulence (FST) with inlet intensity levels between 0.5% and 6%. Such flows were referred to as boundary-layer bypass transition in the narrow sense (also see Figure 1) in Wu *et al.* (2017) to distinguish them from bypass transition arising from other sources, such as separation bubble, roughness element, or very high-level FST.

Conventionally, only one data set, the experiment of Roach (1990), is used for benchmarking and evaluating transition prediction models. Roach (1990) reported wind-tunnel experiments in three conditions: case T3A, with upstream turbulence intensity 3.5%; case T3B, with upstream turbulence intensity 6.5%; and case T3A-, with upstream turbulence intensity 0.8%. One salient feature of their experiments is that their skin-friction coefficient  $C_f$  data collapse onto the Blasius solution prior to laminar-layer breakdown. Several transition models developed since then have used Roach's skin-friction coefficient  $C_f$  data for benchmarking and tuning [for instance, see Westin & Henkes (1997), Suzen & Huang (2000), Menter *et al.* (2006), Durbin (2012), Ge *et al.* (2014), Menter *et al.* (2015), among

<sup>†</sup> Royal Military College of Canada, Canada

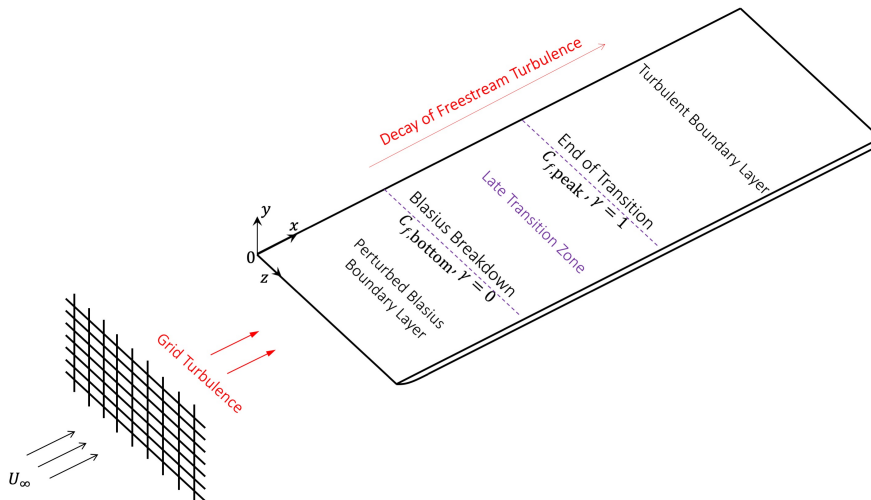


FIGURE 1. Sketch of boundary-layer bypass transition in the narrow sense.

many others].

Notwithstanding its wide popularity, several notable drawbacks are still associated with the data set of Roach (1990). First, the downstream development history of the FST length scales over the boundary layer was not reported. Second, their  $C_f$  data were estimated indirectly from momentum balance rather than directly from near-wall velocity gradient. Third, during transition between  $C_f$  departing from the laminar distribution and attaining the turbulent level, there are only three skin-friction data points in case T3A, and only one data point in case T3B. Fourth, there is a wide gap between T3A- and Case T3A, with no experimental cases covering scenarios in which the inlet freestream turbulence intensity (FSTI) is between 1.0% and 3%. This indicates a need to generate a more thorough database for transition model benchmarking and calibration.

Several direct numerical simulation (DNS) databases exist on this matter. However, we highlight some potential limitations of these works. First, some previous DNSs attempted to reproduce the Roach & Brierley experiments; however, the DNS FST decayed much faster than that in the experiment, potentially due to limited grid resolutions and domain sizes, especially in the freestream. Second, the skin friction in some of the existing DNSs departs from the Blasius solution profile earlier than desired in the early transitional region. The present study aims to improve upon some of these limitations. Overall, the objectives of this study are as follows: (i) construct a DNS database for benchmarking RANS predictions of bypass transition in the narrow sense, (ii) calibrate classical transition correlation and develop an improved correlation connecting intermittency factor, Reynolds number and FSTI, and (iii) perform RANS transition calculations and compare the predictions with the present DNS benchmark.

## 2. Method

We performed five DNS cases of boundary-layer bypass transition in the narrow sense. Additionally, RANS calculations were performed to model the DNS cases. Inlet FST levels in the five DNS cases of boundary-layer bypass transition in the narrow sense are

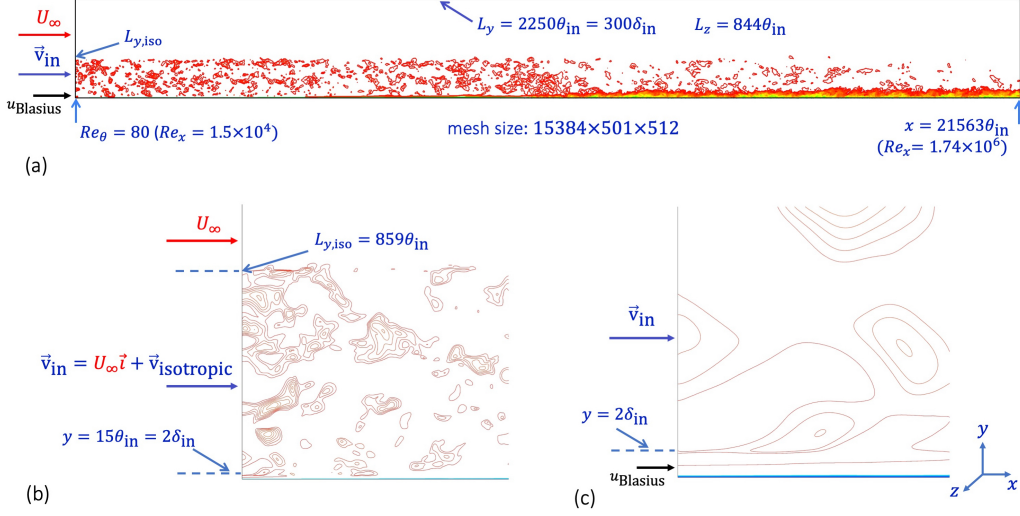


FIGURE 2. Illustration of boundary-layer DNS design using contours of streamwise velocity  $u$  over a random  $xy$ -plane where blue and red colors indicate  $u = 0$  and  $u = U_\infty$ , respectively. (a) Full view; (b) zoomed-in view near the inlet; (c) further zoomed-in view near the inlet.

0.75% for WM075, 1.5% for WM150, 2.25% for WM225, 3.0% for WM300 and 6.0% for WM600.

For the WM-series DNS cases, the domain size, mesh size, inflow turbulence  $\vec{v}_{\text{isotropic}}$  generation, boundary condition and numerical method are exactly the same as those described in Wu *et al.* (2017). Figure 2 recapitulates some of the important parameters defining the DNS. FST is introduced at the inlet over the wall-normal range  $15\theta_{\text{in}} < y < L_{y,\text{iso}}$ , above which is only the far upstream uniform flow  $U_\infty$  without fluctuation, and below which is only the Blasius velocity profile without fluctuation.  $\theta_{\text{in}}$  is the constant inlet boundary layer momentum thickness. At the streamwise exit, domain height  $L_y$  is equivalent to 24.31, 9.05, 7.36, 7.24, and 6.66 local boundary-layer thickness  $\delta_{\text{exit}}$  in WM075, WM150, WM225, WM300 and WM600, respectively. This domain height is larger than that in many previous DNS studies.  $L_{y,\text{iso}}$  is equivalent to 9.28 and 2.54 local boundary-layer thickness  $\delta_{\text{exit}}$  in WM075 and WM600, respectively. At the top of the computational domain, in the WM-series, the following boundary conditions were applied:  $v = v_{\text{Blasius}}$ ,  $\partial u / \partial y = \partial v / \partial x$ ,  $\partial w / \partial y = \partial v / \partial z$ . Given the substantial distance between the top surface and the wall, we expect that the effect of the top boundary condition on boundary-layer development should be minimal.

Figure 3 shows the streamwise and spanwise grid resolutions measured by the local Kolmogorov length scale  $\eta = (\nu^3 / \varepsilon)^{1/4}$  in WM150, where  $\nu$  is the kinematic eddy viscosity of the fluid, and  $\varepsilon$  is the local rate of viscous dissipation of turbulence kinetic energy evaluated from the DNS. Wall-normal distributions of  $\Delta x / \eta$  and  $\Delta z / \eta$  at two representative streamwise stations are shown:  $Re_\theta = 500$  during the transition and  $Re_\theta = 2000$  in the fully turbulent region. It is seen from Figure 3(a) that during the transition, the horizontal plane grid resolutions are less than  $2\eta$ , and after transition, they are less than  $4\eta$ . The near-flat profiles at larger values of  $y^+$  indicate the freestream region outside the boundary layer. Figure 3(b) shows the normalized wall-normal resolution  $\Delta y / \eta$  and the temporal resolution  $\Delta t / \tau_\eta$  in WM150, where  $\tau_\eta = (\nu / \varepsilon)^{1/2}$  is the local Kolmogorov timescale. It is seen that the temporal resolution is less than  $\tau_\eta$ . Inside the boundary

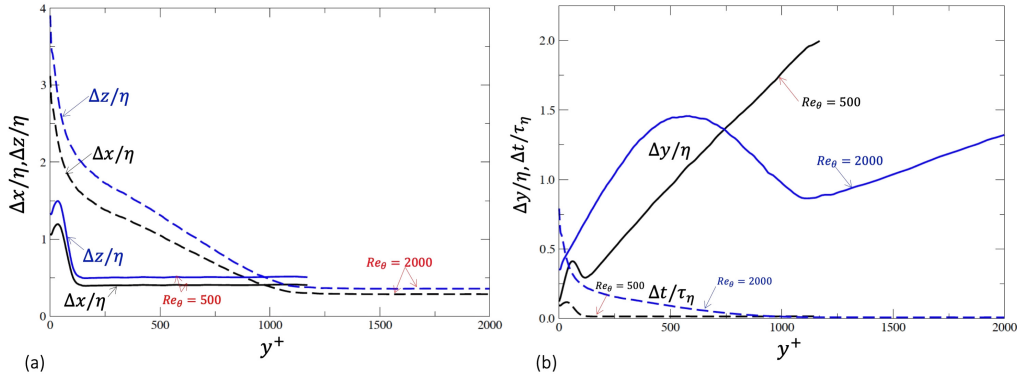


FIGURE 3. DNS spatial and temporal resolutions measured by local Kolmogorov scales in WM150.

layer, the wall-normal resolution is less than  $1.5\eta$ . In the freestream region, even with mesh stretching, the wall-normal resolution is less than  $2\eta$ .

### 3. DNS benchmarks for transition prediction

We processed the statistics from the WM-series DNS cases into a 1D line plot format, and the resulting data files are named as independent variable versus dependent variable at xxx location. They can be accessed from the [Center for Turbulence Research website](#). They can also be downloaded [from Google-Drive](#). The five folders named with stats-WMxxx contain streamwise variations of  $C_f$ , boundary-layer thickness  $\delta$ , displacement thickness  $\delta^*$ , shape factor  $H$ , intermittency factor (for discussion, see Section 7), wall-pressure fluctuation  $p'_{w,rms}$ , wall-shear stress fluctuation  $\tau'_{w,rms}$ ; the independent variables are either the streamwise Reynolds number  $Re_x = xU_\infty/\nu$ , the momentum-thickness Reynolds number  $Re_\theta = \theta U_\infty/\nu$  or the boundary-layer turbulent Reynolds number  $Re_\tau = u_\tau \delta/\nu$ , where  $u_\tau$  is the friction velocity. The five folders also contain wall-normal variations of  $\bar{u}$ ,  $u'_{rms}$ ,  $v'_{rms}$ ,  $w'_{rms}$ ,  $\overline{u'v'}$ ,  $p'_{rms}$ , and total shear stress  $\tau$  with either outer variable  $y/\delta$  or wall-unit  $y^+$  at selected streamwise stations covering the early, late and post-transition stages (overbar indicates averaging). The statistics were sampled during the DNS runs on the fly at every time-step and the sampling duration lasted two flow-through times from the inlet to the exit. Comparisons of mean and second-order statistics, especially comparisons of the rate of dissipation, demonstrate that the present statistics are of good quality (Wu et al. 2017).

#### 3.1. Skin-friction profiles

Some of the generated statistical quantities are presented herein for reference. In particular, Figure 4(a) shows  $C_f$  as a function of  $Re_x$ . Starting from the inlet, all five cases show an extended range in which  $C_f$  remains in close agreement with, and collapses onto, the Blasius solution, even in the highest-level FSTI case WM600. Departure from the Blasius is only visible shortly upstream of the minimum  $C_f$  location. The case WM075 has not completed its transition process by the exit of the present computational domain. Variations of  $C_f$  with  $Re_\theta$  are shown in Figure 4(b). Shortly after reaching a peak plateau, the WM225  $C_f$  profile collapses onto that of the WM300, suggesting the downstream WM225 boundary layer is turbulent with a small lingering transitional effect.

Similarly, shortly after reaching its peak plateau, the WM150 profile collapses onto

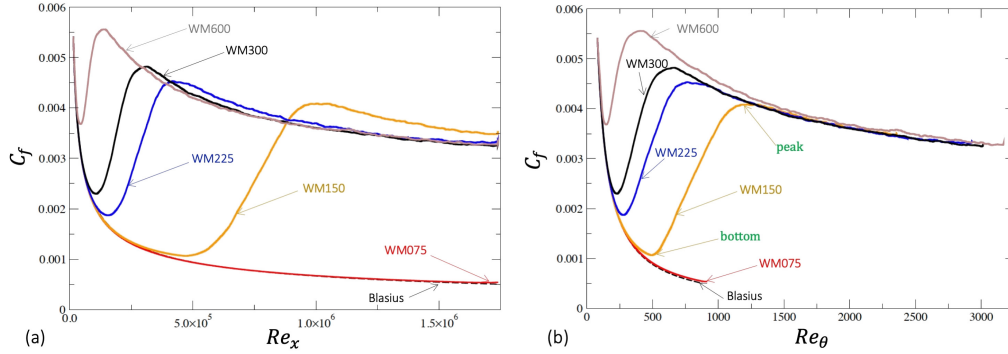


FIGURE 4. Skin-friction coefficient as a function of (a) streamwise Reynolds number and (b) momentum-thickness Reynolds number in the five boundary-layer DNS cases.

those of WM225 and WM300, implying the downstream WM150 boundary layer is turbulent with a small transitional effect (the peak plateau of skin friction indicates the completion of transition). After the transition in the turbulent flow region, the WM600  $C_f$  profile still does not collapse onto the profiles of the other three cases, indicating that its higher FST level causes noticeable disturbances to the viscous sublayer of the turbulent boundary layer underneath. Although not shown, the shape factor,  $H$ , for the WM600 case exhibited a precipitous drop near the inlet, indicating a strong disturbance on the boundary layer by the high-level FST. Due to these reasons, we hypothesize the upper limit of boundary-layer bypass transition in the narrow sense as approximately FSTI 6%, beyond which transition is rather immediate.

#### 4. Improved intermittency correlation and comparison with literature

Building upon the comprehensive DNS database described in previous sections, we developed a new correlation for predicting boundary-layer transition. The correlation is of the form

$$Re_\theta = f(\text{FSTI}, \frac{\Lambda_x}{\delta}, \gamma), \quad (4.1)$$

where the input three variables are the free stream turbulence intensity, the freestream turbulence integral length scale normalized by the boundary-layer thickness, and the desired intermittency factor to demarcate as the transition location, respectively. Prior work (Fransson & Shahinfar 2020) has shown that transition location can be highly sensitive to length scales associated with freestream turbulence. In developing our new transition correlation, we observed that the classical correlation of Abu-Ghannam & Shaw (1980)

$$Re_\theta = 163 + \exp(6.91 - \text{FSTI}), \quad (4.2)$$

accurately predicts the location where  $\gamma = 0$  in our DNS data across the various freestream turbulence intensities, shown in Figure 5(a). Using this, we designed the functional form to ensure that it collapses to a form similar to Abu-Ghannam and Shaw's relation when

$\gamma = 0$  by specifically forcing it to take the form

$$Re_x = P_1 \left( \frac{\Lambda_x}{\delta} \right) \cdot \exp(P_2(\gamma)) \cdot g(\text{FSTI}), \quad (4.3)$$

where  $\Lambda_x$  is the the freestream turbulence integral length scale,  $P_1$  and  $P_2$  are polynomial functions, and  $g$  is a function similar to Eq. (4.2). Note that we are fitting for the transition value of  $Re_x$ , principally because this is the value most commonly reported in the literature. Moreover, it is important to highlight that this equation is valid only for  $\gamma \in [0, 1]$ , as this is the range of sensible values for the intermittency function. Curve fitting tests demonstrated that the fitting cubic polynomials in Eq. (4.3) for  $P_1$  and  $P_2$  were sufficient to predict transition. Transition location predictions from the correlation in Eq. (4.3) are shown in Figure 5(b), demonstrating a collapse between both DNS and experimental results. The functions used to generate this collapse are

$$P_1 \left( \frac{\Lambda_x}{\delta} \right) = -8.676 \cdot 10^{-4} \left( \frac{\Lambda_x}{\delta} \right)^3 + 7.490 \cdot 10^{-2} \left( \frac{\Lambda_x}{\delta} \right)^2 + 0.198 \left( \frac{\Lambda_x}{\delta} \right) + 190.5, \quad (4.4)$$

$$P_2(\gamma) = 1.68\gamma^3 - 2.83\gamma^2 + 1.91\gamma + 3.15, \quad (4.5)$$

and

$$g(\text{FSTI}) = 14.36 - \exp(6.55 - 1.45\text{FSTI}). \quad (4.6)$$

Further, we can use the predicted value of the transition Reynolds  $Re_c$  number from Eq. (4.3) to replot the skin-friction profiles of Figure 4(b). By modifying the  $y$ -axis to a laminar scaling component,  $Re_\theta^{-1}$ , and a turbulent scaling component,  $Re_\theta^{-3/4}$ , and by plotting against  $Re_\theta/Re_c$ , we can fully collapse the skin-friction profiles as seen in Figure 6. Successfully modeling the full transition region with Eq. (4.3) demonstrates that the correlation has the potential to be incorporated into a full transition model.

## 5. RANS predictions of the DNS cases

Here we present accompanying RANS calculations of the DNS cases. These simulations were computed using OpenFOAM's simpleFoam solver. The  $k - \omega$  shear-stress transport (SST) turbulence model (Menter 1994) and  $\gamma - Re_\theta$  (Langtry & Menter 2005) transition model are used for all cases. The size of the computational domain is identical to the one used in the DNS. At the inlet, a laminar Blasius velocity profile was prescribed to match the conditions of the DNS. A grid convergence study was performed and convergence was achieved at  $y^+ < 1$  for all simulations.

This set of turbulence and transition models require inlet boundary condition values for  $k$ ,  $\omega$ ,  $\gamma$ ,  $Re_{\theta_i}$ , and  $\nu_t$ . Details on how to set these boundary conditions at the inlet of the computational domain can be found in Langtry & Menter (2009). The equation for the boundary condition for  $\omega$  is given by Eq. (5.1) where  $C_\mu = 0.09$ . This equation leaves a free parameter, a reference length scale  $\mathcal{L}$ , associated with the turbulence.

$$\omega = \frac{\sqrt{k}}{C_\mu^{0.25} \mathcal{L}} \quad (5.1)$$

Implementation differences of the  $k - \omega$  SST model can lead to different recommended values of  $\mathcal{L}$ . For example, in wall-bounded flows ANSYS recommends setting  $\mathcal{L} = 0.4\delta_{99}$  (ANSYS 2009) while COMSOL recommends  $\mathcal{L} = 0.09\delta_{99}$  (COMSOL 2018). Overall, it

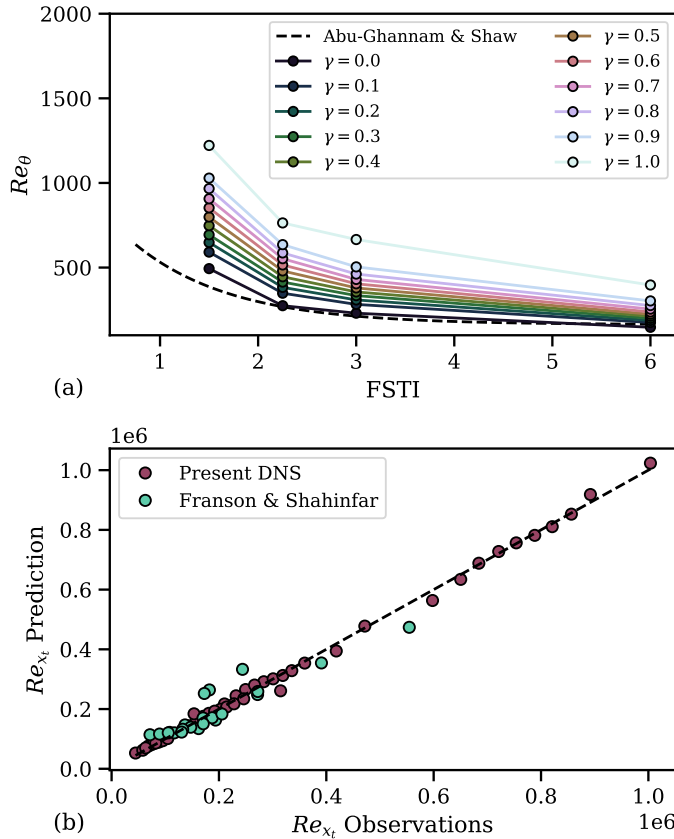


FIGURE 5. (a) Transition location measured in  $Re_\theta$  plotted against the inlet freestream turbulence intensity level. (b) Comparing transition prediction results from Eq. (4.3) to measured results from present simulations and the experimental data set of Fransson & Shahinfar (2020). The experimental data set has a variety of conditions for FSTI and  $\Lambda_x$ . The transition location is always at  $\gamma = 0.5$ . For simulations, we report transition locations from the present DNS for  $\gamma = 0.1n$  for  $0 \leq n \leq 10$ .

was found that in OpenFOAM the value of this parameter that best reproduces the DNS skin-friction profiles across all cases is  $\mathcal{L} = \delta_{99}$ . The skin-friction curves generated from  $\mathcal{L} = \delta_{99}$  are shown in Figure 7. We note that for this choice of length scale used in the boundary condition, the WM600 case is fully turbulent throughout the whole computational domain and does not capture the onset of transition. We emphasize that it is possible to predict the onset of transition at the 6% FSTI level but at the expense of worsening all other predictions. Our testing has shown that there is sensitivity in the location of transition to the value of  $\mathcal{L}$  chosen. Figure 8 shows the sensitivity in  $C_f$  for FSTI = 1.5% for RANS simulations using  $\mathcal{L} = \delta_{99}$ ,  $\mathcal{L} = 0.4\delta_{99}$ , and  $\mathcal{L} = \Lambda_x$ . We see that both the location of transition and the magnitude of the skin-friction rise can be affected by the value of  $\mathcal{L}$  that is specified. This sensitivity demonstrates a lack of predictiveness in RANS-based transition modeling.

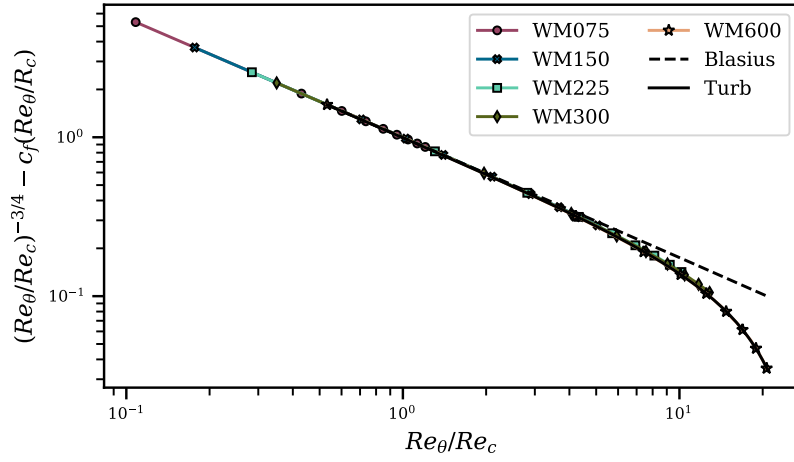
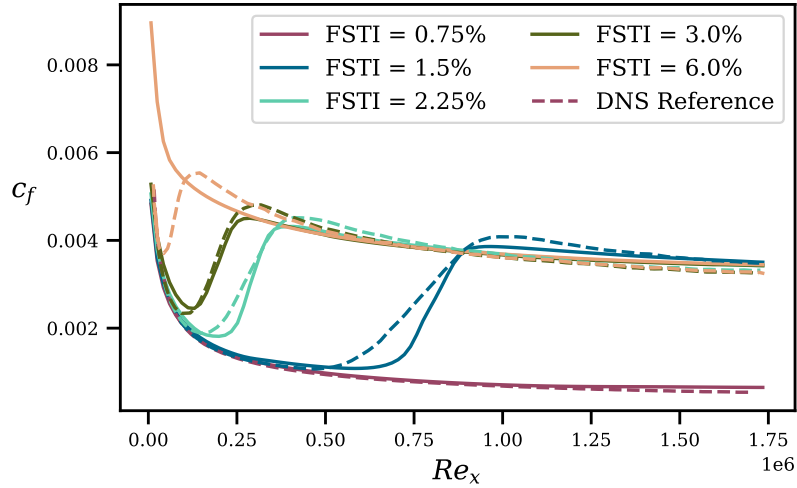


FIGURE 6. Collapsed skin-friction profiles.

FIGURE 7. Solid lines depict skin-friction versus  $Re_x$  for RANS results and dashed lines depict the corresponding DNS results. The length scale used in the boundary condition for  $\omega$  for these results is  $\mathcal{L} = \delta_{99}$ .

## 6. Conclusions

A new set of comprehensive DNS benchmarks of bypass transition with varying levels of inlet freestream turbulence intensity have been computed. Detailed statistics and descriptions of the length scales and dissipation are provided. The full database is available on the CTR website for modelers to take advantage of. Additionally, a new transition correlation has been developed using this DNS database. It builds upon the correlation of Abu-Ghannam and Shaw and is modified to include information about the length scale of the freestream turbulence and the desired intermittency value to denote transition. This correlation has been shown to agree with existing experimental data and was used to collapse the DNS skin-friction profiles onto a single curve. Finally, accompanying RANS simulations were conducted using OpenFOAM. These calculations demonstrate

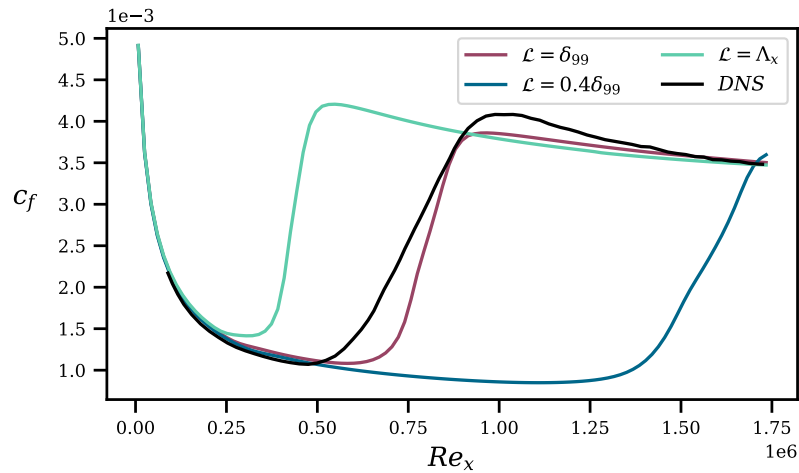


FIGURE 8. Skin-friction versus  $Re_x$  results for RANS computations at FSTI = 1.5%. The large sensitivity in the transition location is tied to the choice of  $\mathcal{L}$  used to set the inlet boundary condition for  $\omega$ .

that state-of-the-art RANS transition modeling (e.g., the  $\gamma - Re_\theta$  model) can be highly sensitive to the length scale used to initialize the turbulence. This DNS database should be useful to RANS researchers in the development of new transition models.

#### REFERENCES

- ANSYS Inc. 2009. *ANSYS FLUENT 12.0/12.1 Theory Guide*.
- COMSOL Inc. 2018. *The CFD Module's User Guide*.
- ABU-GHANNAM, B. & SHAW, R. 1980 Natural transition of boundary layers—the effects of turbulence, pressure gradient, and flow history. *J Mech Eng Sci* **22**, 213–228.
- DICK, E. & KUBACKI, S. 2017 Transition models for turbomachinery boundary layer flows: a review. *Int. J. Turbomach., Propulsion, and Power* **2**, 4.
- DURBIN, P. 2012 An intermittency model for bypass transition. *Int. J. Heat. Fluid. Fl* **36**, 1–6.
- DURBIN, P. A. 2018 Some recent developments in turbulence closure modeling. *Annu. Rev. Fluid. Mech.* **50**, 77–103.
- FRANSSON, J. H. & SHAHINFAR, S. 2020 On the effect of free-stream turbulence on boundary-layer transition. *J. Fluid. Mech.* **899**, A23.
- GE, X., AROLLA, S. & DURBIN, P. 2014 A bypass transition model based on the intermittency function. *Flow. Turbul. Combust.* **93**, 37–61.
- LANGTRY, R. & MENTER, F. 2005 Transition modeling for general CFD applications in aeronautics. In *AIAA Pap. 2005-522*.
- LANGTRY, R. B. & MENTER, F. R. 2009 Correlation-based transition modeling for unstructured parallelized computational fluid dynamics codes. *AIAA J.* **47**, 2894–2906.
- MENTER, F. R. 1994 Two-equation eddy-viscosity turbulence models for engineering applications. *AIAA J.* **32**, 1598–1605.

- MENTER, F. R., LANGTRY, R. & VÖLKER, S. 2006 Transition modelling for general purpose CFD codes. *Flow. Turbul. Combust.* **77**, 277–303.
- MENTER, F. R., SMIRNOV, P. E., LIU, T. & AVANCHA, R. 2015 A one-equation local correlation-based transition model. *Flow. Turbul. Combust.* **95**, 583–619.
- ROACH, P. 1990 The influence of a turbulent free-stream on zero pressure gradient transitional boundary layer development part I: test cases T3A and T3B. *Numerical Simulation of Unsteady Flows and Transition to Turbulence*, (eds O. Pironneau, W. Rodi, I.L. Rhyming, A. M. Savill & T.V. Truong). pp. 319–347. Cambridge, UK: Cambridge University Press.
- SUZEN, Y. & HUANG, P. 2000 Modeling of flow transition using an intermittency transport equation. *J. Fluids Eng.* **122**, 273–284.
- WESTIN, K. & HENKES, R. 1997 Application of turbulence models to bypass transition. *J. Fluid Eng.* **119**, 859–866.
- WU, X., MOIN, P., WALLACE, J. M., SKARDA, J., LOZANO-DURÁN, A. & HICKEY, J.-P. 2017 Transitional–turbulent spots and turbulent–turbulent spots in boundary layers. *PNAS* **114**, E5292–E5299.